RSC Advances

PAPER

The sponge silicatein-interacting protein silintaphin-2 blocks calcite formation of calcareous sponge spicules at the vaterite stage

Cite this: *RSC Adv.*, 2014, **4**, 2577

Werner E. G. Müller,*[a] Meik Neufurth,[a] Ute Schlossmacher,[a] Heinz C. Schröder,[a] Dario Pisignano[b] and Xiaohong Wang*[a]

Ca-carbonate, the inorganic matrix of the spicules from the calcareous sponges, is formed as the result of an enzyme-catalyzed reaction with the carbonic anhydrase [CA] as a decisive component. The growth and the morphology of the spicules are genetically controlled, and are taxon-specific. In the present study it is shown that the silicatein-interacting protein silintaphin-2 is present at the surface of the siliceous spicules of the demosponge *Suberites domuncula* and prevents the association of calcareous crystals synthesized *in vitro* to these skeletal elements. Silintaphin-2 comprises a Ca^{2+}-binding domain that is formed by a 22 amino acid-long peptide, N-DDDSQGEIQSDMAEEEDDDNVD-C. This very acidic 22-meric peptide, termed D/E-peptide, is shown to decelerate the *in vitro* synthesis of calcite through blocking the transformation of amorphous Ca-carbonate to the crystalline morph calcite at the level of vaterite. This effect is seen at a molar ratio of D/E-peptide : Ca^{2+} of 1 : 5000. During the deposition of Ca-carbonate the peptide becomes incorporated into the crystallites. Determinations of the mechanical characteristics of the formed Ca-carbonate deposits revealed a hardness of 1.98 ± 0.31 GPa (calcite) and 1.38 ± 0.39 GPa (vaterite), an elastic modulus of 72.83 ± 11.68 GPa (calcite) and 39.13 ± 8.04 GPa (vaterite) and a creep of 5.44 ± 1.15 (calcite) and 9.95 ± 1.60 (vaterite) per maximal depth (%). It is concluded that the D/E-peptide interferes with the Ca^{2+} ions within the growing vaterite crystals and freezes this unstable phase formed during calcite formation. It is postulated that proteins, like silintaphin-2 with its Ca^{2+}-binding domain D/E-peptide, are involved in the taxon-specific control of the synthesis of the inorganic matrix of the sponge spicules.

Received 17th September 2013
Accepted 5th November 2013

DOI: 10.1039/c3ra45193c

www.rsc.org/advances

1. Introduction

Calcium carbonate (Ca-carbonate) is prevalent both as a geological mineral and as a biomineral. It occurs both in an amorphous (ACC) and a crystalline state (CCC) and this feature makes this mineral to a suitable material that can be molded to form intricately architectured biomineral structures, like in calcareous sponges,[1] mollusk shells[2] or radiolarians.[3] Ca-carbonate exists in five different crystalline polymorphs, the hydrated phases (monohydrocalcite and ikaite) and the anhydrous phases (vaterite, aragonite, and calcite). In the presence of water or when heated, ACC is transformed into one of the CCC calcium carbonate forms, following the energetically downhill sequence vaterite–aragonite–calcite.[4] In organisms, having a Ca-carbonate-based skeleton, ACC is the precursor of the complex calcite, aragonite and vaterite structures of shells, spines, teeth, and spicules.[5] The skeletal elements of the calcareous sponges are almost completely composed of calcite, besides of a low content of aragonite.[6] Based on the results of a series of biochemical, optical and spectroscopic studies, it is well accepted that the spicules from calcareous sponges can be described best as a single crystal (reviewed in: ref. 7).

The biochemical routes by which the calcitic skeletal elements of metazoans are formed are not yet conclusively elucidated (see: ref. 8). Besides of genes encoding for non-enzymatic proteins, those encoding for the enzymes carbonic anhydrase (CA), alkaline phosphatase, peroxidase, tyrosinase and chitin synthase are highly expressed during the development of the mollusk shell. There are especially the CAs, enzymes that catalyze the synthesis of bicarbonate *via* hydration of carbon dioxide, which have been implicated not only in the formation of the mollusk shell (see: ref. 8), but also in the synthesis of the Ca-carbonate spicules of the calcareous sponges,[9] of the coral skeleton[10,11] or of the echinoderm sclerites.[12] CA-derived bicarbonate can undergo Ca-carbonate formation if Ca^{2+} ions are available, *e.g.* after transport *via*

[a]*ERC Advanced Grant Research Group at the Institute for Physiological Chemistry, University Medical Center of the Johannes Gutenberg University Mainz, Duesbergweg 6, D-55128 Mainz, Germany. E-mail: wmueller@uni-mainz.de; wang013@uni-mainz.de; Fax: +49 6131-39-25243; Tel: +49 6131-39-25910*

[b]*National Nanotechnology Laboratory of Istituto Nanoscienze-CNR and Dipartimento di Matematica e Fisica "Ennio De Giorgi", Università del Salento, via Arnesano, I-73100 Lecce, Italy*

transmembrane pumps (Ca-ATPases). The involvement of enzymatic reaction(s) of the intermediary metabolism as regulatory step(s), occurring at crossing points of different metabolic pathways, is an almost general concept to adjust and to maintain a balanced regulation of the concentrations of the respective (organic) metabolites involved. In the case of biomineralization processes, it can be postulated that the (in)organic substrates/matrices required for at least some of these polymerization/deposition processes are supplied in an enzyme-mediated way, while the subsequent form and morphology formation is under the control of non-enzymatic structure-guiding proteins. This concept has for the first time been proven experimentally for the synthesis of the siliceous sponge spicules (see: ref. 13 and 14). The amorphous soft matter, the polymeric biosilica, is supplied by the enzyme silicatein, while the subsequent steps of structure and morphology formation are guided by oligo-/polymeric self-assembled silicatein molecules and filaments.[15] During this process of "precision biosilica molding" biosilica is assumed to be pressed into a pre-formed collagen cast. Furthermore, during silica rod formation, the reaction water that is formed during siloxane bond formation is extracted/extruded from the initial biosilica product.[16]

A similar enzymatic mechanism, as described for the biosilica/spicule formation, has been proposed to exist for the formation of Ca-carbonate based skeletal elements. Very recently we demonstrated that the enzyme, CA, is crucially involved in the synthesis of calcareous spicules.[17,18] Bicarbonate ions, provided by the CA, undergo precipitation in the presence of Ca^{2+} ions, into the fairly insoluble form ACC that subsequently undergoes phase transformation into the CCC forms during which the water content gradually decreases.[19] While for mollusk shell formation a series of non-enzymatically acting peptides have been described to be involved in the control of Ca-carbonate deposition (see: ref. 8) only a few data exist for the calcareous sponge spicules. It had been described that the calcareous spicules, isolated from the calcareous sponge species *Sycon*, *Kebira* and *Clathrina* contain a dispersed proteinaceous organic matrix, rich in aspartic acid (Asp, D) and glutamic acid (Glu, E).[20] The detailed reaction sequence by which those peptides participate in CCC formation is not known. Especially the acidic amino acids, D and E, within a (glyco)protein are considered to be the active sites controlling biomineralization. This process is certainly genetically controlled, and in turn conducted by the expressed proteins either directly or indirectly, *e.g.* by protein/enzyme-controlled synthesis of non-proteinaceous, organic molecules. They are located at the organic/inorganic interface of the biomineralized tissue.[21,22]

In a recent study we described that the siliceous spicules from the demosponge *Suberites domuncula* are not able to associate with Ca-carbonate crystallites formed during *in vitro* biocalcite formation.[17,18] In continuation of this observation we report now that silintaphin-2, a silicatein-interactor which comprises a high binding affinity to Ca^{2+},[23] is present at the surface of the spicules. The major Ca^{2+}-binding site of silintaphin-2 has been narrowed down to the oligopeptide stretch aa_{51} to aa_{72}; this 22-mer has the sequence N-DDDSQGEIQSDMAEEEDDDNVD-C and has been termed D/E-peptide. We demonstrate that this D/E-peptide slows down the CA-driven Ca-carbonate formation and prevents transformation into calcite from ACC by freezing the reaction at the intermediate morph vaterite. It is postulated that proteins, provided with a high Ca^{2+} binding affinity that surround the siliceous spicules are involved in the species-specific acceptance/rejection of spicules in sponges.

2. Material and methods

2.1. Materials

Carbonic anhydrase (bovine cytosolic CA-II; C2624; specific activity ≥3500 W-A units mg^{-1} protein) was purchased from Sigma (Taufkirchen; Germany). This enzyme (EC number 4.2.1.1) has been purified from bovine erythrocytes. Polyclonal antibodies (P00921), raised in rabbits against this CA-II, were from Merck-Millipore (Billerica, MA).

2.2. Sponge specimens and their spicules

Specimens of the marine sponges *Sycon raphanus* (Porifera, Calcarea, Leucosolenida) and *Suberites domuncula* (Porifera, Demospongiae, Hadromerida) were collected in the Northern Adriatic near Rovinj (Croatia). They were kept in aquaria in Mainz (Germany) at a temperature of 17 °C for more than 12 months.[24] The spicules were isolated and purified as described.[9,14]

2.3. Silintaphin-2

The silintaphin-2 sequence is deposited in the NCBI database under the accession number CBW45489.[23] Polyclonal antibodies (PoAb-aSiphn-2-01) were raised against the recombinant silintaphin-2 in BALB/c mice;[23] preimmune serum was collected as a control.

2.4. Immunohistology

Immunohistological analysis was performed with 8 μm-tissue slices through *S. domuncula* tissue.[25] The samples were fixed in paraformaldehyde and incubated with the primary antibodies PoAb-aSiphn-2-01 (dilution: 1 : 5000) in blocking solution while shaking at 4 °C overnight. The immunocomplexes were visualized with Cy5-conjugated goat anti-mouse immunoglobulin G (IgG). Parallel slices were stained with DAPI (4′,6-diamidino-2-phenylindole). Finally, the slices were inspected with an Olympus AHBT3 microscope under immunofluorescence light at an excitation light wave-length of 647 nm (Cy5-stained structures) or of 490 nm (DAPI). Isolated *S. domuncula* spicules were reacted in the same way with the PoAb-aSiphn-2-01 antibodies.

2.5. Ca-carbonate precipitation assay

Precipitation experiments, to obtain Ca-carbonate deposits, were performed in diffusion chambers as described.[26] This "dessicator method" is based on the diffusion of CO_2 vapor, generated from a NH_4HCO_3 (Sigma; ≥ 99.0%) solution in the lower compartment, into the upper compartment of the chamber which contained in a 8-well Lab-Tek II chamber slide (Fisher Scientific, Schwerte; Germany) 500 μL of 50 mM $CaCl_2$ (Sigma; ≥99.9%). The pH value of the solution was buffered with 30 mM TRIS [Tris(hydroxymethyl)-aminomethane] to pH

8.4; the temperature was set to 22 °C. Where indicated, bovine CA was added at a final concentration of 35 W-A units (10 μg)/500 μL of $CaCl_2$.

The extent of Ca-carbonate formation was quantitated on the basis of the consumption Ca^{2+} ions in the solution by EDTA titration.[27]

In one series of experiments the round-shaped deposits were treated with acetic acid to dissolve the Ca-carbonate matrix. The particles are transferred on a microscope slide into a solution of 1% [v/v] of acetic acid and treated for up to 20 min (20 °C). Subsequently, the samples were washed with distilled water and stained with 1% [w/v] of Coomassie Brilliant Blue G-250 (Sigma).

2.6. D/E-peptide

The peptide N-DDDSQGEIQSDMAEEEDDDNVD-C (M_r 2.47 kDa), spanning the oligopeptide stretch aa_{51} to aa_{72} of silintaphin-2 was synthesized by solid phase peptide synthesis (PANATecs GmbH, Heilbronn; Germany). This peptide was, where indicated, added at a concentration of 30 μg mL^{-1} (≈10 μM).

2.7. Microscopic inspections

The light microscopic (LM) images of the Ca-carbonate deposits were taken either with an Olympus AHBT3 microscope or a light digital microscope (VHX-600 Digital Microscope) from KEYENCE (Neu-Isenburg; Germany), equipped with a VH-Z25 zoom lens.

For the scanning electron microscopic (SEM) analyses, a HITACHI SU 8000 (Hitachi High-Technologies Europe GmbH, Krefeld; Germany) was employed at low voltage (<1 kV; analysis of near-surface organic surfaces).[28]

2.8. Fourier transform infrared (FT-IR) spectrometry

FT-IR spectrometry was performed as described.[29] Samples were powderized in a mortar with pestle. The spectra were recorded from 550 to 4000 cm^{-1} using a Varian 660-IR spectrometer (Agilent Technologies, Böblingen; Germany), equipped with a Specac Golden-Gate diamond ATR unit (Specac Ltd, Orpington; United Kingdom). For each spectrum 36 scans with a spectral resolution of 4 cm^{-1} were carried out. For the analysis of the spectra the Resolutions Pro 5.2.0 software package was used (Agilent). From the spectra recorded the background data (without sample) were subtracted. Using this method[29] the absorption band(s), characteristic for calcite 873 cm^{-1} and 713/711 cm^{-1}, for vaterite 875 cm^{-1} and 745/744 cm^{-1} and for aragonite 858 cm^{-1}, 713 cm^{-1} and 700 cm^{-1} were recorded.

2.9. Nanoindentation studies

Nanoindentation experiments were carried out with a NanoTest Vantage system (Micro Materials Ltd, Wrexham; UK) using continuous depth-sensing indentation[30] and a three-sided Berkovich diamond. Onto each sample ten indents were conducted at a temperature of 30 °C with a maximum depth of 500 nm and a maximum load of 10 mN. The loading as well as the unloading was set to 30 s applying a maximal load of 40 s. For the first contact the initial load was set to 0.05 mN and the surface approach velocity was constant at 0.2 μm s^{-1}. The minimum spacing between the indents was set to 10 μm. The calculations of the hardness and the reduced modulus were conducted as described.[30] By fitting a power-law function to the unloading segment of a load–displacement curve, the initial unloading stiffness and the projected contact area was calculated. The slope of unloading curve at peak load was used to determine the contact depth of an indent. The calculations were performed with the software NanoTest Platform Four V.40.08 (Micro Materials Ltd).

2.10. Additional methods

For the quantification of protein, the described Bradford method[31] was used with the indicator Roti-Quant (Roth). The results were statistically evaluated.[32]

3. Results

3.1. The D/E-peptide

The 138 amino acids (aa) long deduced silintaphin-2 sequence comprises three potential Ca^{2+}-binding sites at aa_{22} to aa_{35}, aa_{44} to aa_{73} and aa_{79} to aa_{91} (Fig. 1A). These sites had been predicted by applying the described algorithm[33] and subsequently confirmed experimentally.[23] They are located within the pronounced helices of the predicted secondary structure of the protein that has been assessed by using the CFSSP: Chu & Fasman secondary structure prediction server (http://www.biogem.org/tool/chou-fasman/). The dominance of the helical regions (64% helix; 30% sheet; and only 5% coil) within the silintaphin-2 sequence indicates that this molecule is a rod-like and inflexible fibrillar protein.[34]

The D/E-peptide selected here, a 22-mer, spans the stretch aa_{51} to aa_{72} within the silintaphin-2 sequence, as marked in Fig. 1A. This peptide has a M_r of 2471.3 and an isoelectric point (p*I*) of 2.99, due to the existence of the negatively charged amino

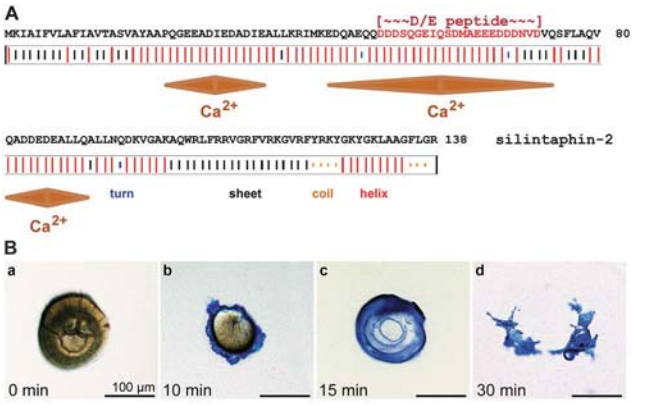

Fig. 1 The D/E-peptide of *S. domuncula* silintaphin-2. (A) The sequence is 138 aa long and comprises three potential Ca^{2+}-binding sites that are delimited by diamonds. The secondary structures (helix [red], sheet [black], coil [brown] and turn [blue]) have been predicted and are highlighted below the sequence. The location of the D/E-peptide is given. (B) The release of the D/E-peptide from the round-shaped deposits after dissolution of the Ca-carbonate matrix. The matrix has been dissolved with acetic acid in a time-dependent manner for 0 to 30 min (Ba to Bd); the peptide scaffold becomes increasingly stained by Coomassie Brilliant Blue.

acids aspartic acids (D) and glutamic acid (E) that are even clustered *DDD*SQG*E*IQS*D*MA*EEEDDD*NV*D*. Prediction analysis[35] reveals that one mole of peptide is able to bind one mole of Ca^{2+} ion. In the Ca-carbonate precipitation experiments, described here, the D/E-peptide was added at a concentration of 30 μg mL^{-1}, which is equivalent to about 10 μM.

3.2. Localization of silintaphin-2 on the surface of *S. domuncula* spicules

The distribution of the spicules within the tissue of *S. domuncula* can be identified by Nomarsky interference contrast optics (Fig. 2A and D). Silintaphin-2 has been localized by immunofluorescence histology using the specific antibodies PoAb-aSiphn-2-01. The immunoreactions revealed a strong staining of the tissue slices at the surfaces of the spicules (Fig. 2B and E). In parallel sections the nuclei of the cells were stained with DAPI (Fig. 2F), in regions that remained unstained in the immunoreactions (Fig. 2E). However, in the latter slices the surfaces of the spicules, scattered within the tissue, brightly lighted up. If isolated spicules were taken for the immunoreaction studies it became evident that the PoAb-aSiphn-2-01 anti-silintaphin-2 antibodies recognize not only the surface of the spicules, but also the axial filament within these skeletal structures (Fig. 2G and H). In two control reactions it was demonstrated that the reactions seen with the PoAb-aSiphn-2-01 antibodies are specific for silintaphin-2, since the corresponding preimmune serum did not react with any structure within the tissue (Fig. 2C), or at the spicules (Fig. 2I).

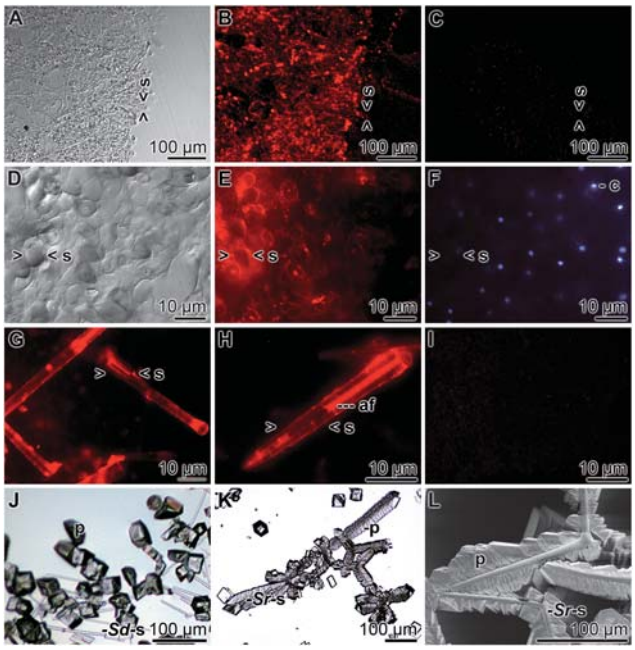

Fig. 2 Localization of silintaphin-2 at the *S. domuncula* spicules; (A to I) LM; (J to L): SEM. Both tissue sections through *S. domuncula* (A to F) and isolated *S. domuncula* spicules (G to I) were incubated with antibodies against silintaphin-2 (PoAb-aSiphn-2-01) and subsequently with Cy5-labelled anti-mouse IgG (B, E, G and H). In (F) the section was reacted with DAPI. In (C) and (I) the corresponding samples were incubated with preimmune serum. The immune-reacted samples were inspected with Olympus AHBT3 microscope under immunofluorescence light at an excitation light wave-length of 647 nm (Cy5-stained structures) or of 490 nm (DAPI). (A and D) The non-stained samples were inspected with Nomarsky interference contrast optics. Some spicules (> <: s) or cells (- c) were labeled. In addition, the axial filament (- af) of one *S. domuncula* spicule is highlighted (H). (J to L) Differential association of Ca-carbonate prisms, formed *in vitro*, to (J) 150 μm long *S. domuncula* oxeae or tylostyle spicules (*Sd*-s) or to (K and L [SEM]) 350 μm long *S. raphanus* triactines (*Sr*-s). The *in vitro*-formed prisms (p) associate only with the *S. raphanus* spicules. The incubation period was 3 h in the presence of CA, and the absence of the D/E-peptide.

3.3. Association of Ca-carbonate deposits with sponge spicules *in vitro*

If the Ca-carbonate precipitation reaction was performed in the presence of CA (35 W-A units per assay) and in the absence of the D/E-peptide, the Ca-carbonate prisms formed *in vitro* do not associate with siliceous spicules from *S. domuncula* (Fig. 2J). However, these *in vitro* formed prisms readily form palisade-like rows of orderly arranged crystals onto the surfaces of spicules from the calcareous sponge *S. raphanus* (Fig. 2K and L). This arrangement of the prisms is highly ordered in a way that, very likely, due to a spatial constraint, only two arrays of aligned crystals become attached to the spicules. These two rows of prisms are facing each other and allow to leave the two remaining planes of the spicule uncovered (Fig. 2L).

3.4. Effect of the D/E-peptide on the Ca-carbonate deposits

Under the conditions outlined under "Material and Methods" two morphologically different deposits are formed in the presence of CA (35 W-A units per assay); first prisms with an average size of 80–120 μm and second round-shaped deposits of similar dimensions (Fig. 3A). In the absence of the D/E-peptide, prisms with a rhombohedral morphology are formed (Fig. 3B and D), while in the presence of 10 μM D/E-peptide round-shaped deposits are synthesized (Fig. 3C and E).

The Ca-carbonate matrix of the round-shaped deposits was dissolved in acetic acid to clarify if the D/E-peptide molecules are incorporated into the inorganic salt deposits. To identify the released peptide the samples were stained with Coomassie Brilliant Blue. As shown in Fig. 1B the peptide became increasingly exposed after dissolution of Ca-carbonate. After a period of 10 min the rim became positively stained for the peptide, while the central region containing the mineralic deposits remained unstained. After a total incubation period of 30 min the inorganic Ca-carbonate was completely dissolved leaving the proteinaceous scaffold behind (Fig. 1B(a to d)).

3.5. Characterization of the Ca-carbonate polymorphs

The hardness, elastic modulus and creep of the two forms of Ca-carbonate deposits, the calcitic prisms (Fig. 4A(a) and Fig. 5A) and the round-shaped vaterite deposits (Fig. 4A(b) and Fig. 5B), were determined by nanoindentation. The hardness is reflecting the resistance of the deposits to plastic deformation, while the elastic modulus represents the elastic deformation of the material following force application. The load–displacement curves for the two Ca-carbonate forms, the calcitic prisms and

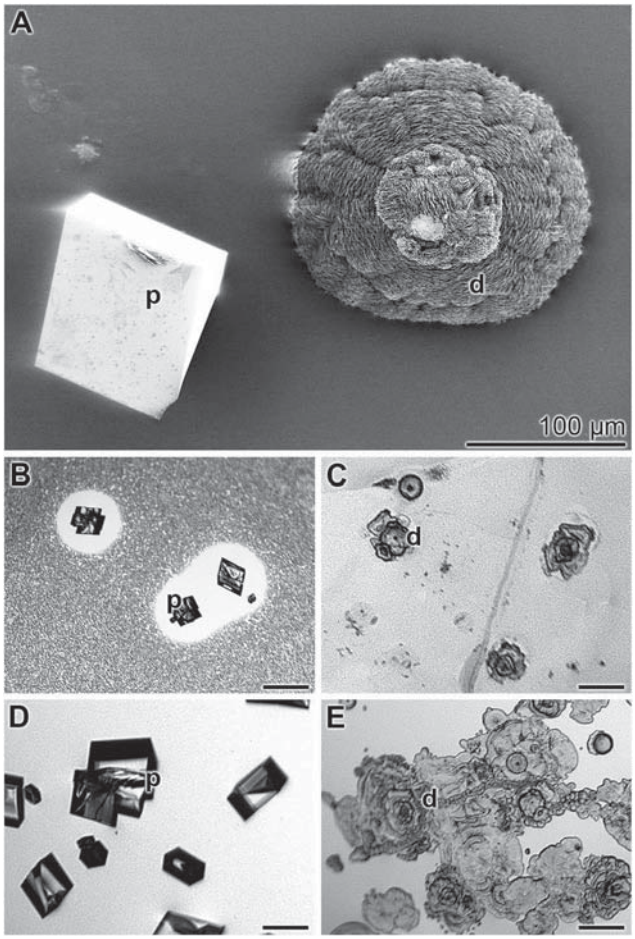

Fig. 3 (A) Morphology of the Ca-carbonate deposits formed *in vitro*, in the "dessicator assay"; the rhombohedral prisms (p) and the round-shaped deposits (d). (B and D) The prisms (p) are formed in the assays containing CA (35 W-A units per assay) and lacking the D/E-peptide, while the round-shaped deposits (d) (C and E) are synthesized in the assays supplemented with CA and 10 μM D/E-peptide, during an incubation period of 60 min (B and C) and of 180 min (D and E). All scale bars measure 100 μm. (A): SEM; (B to E): TEM.

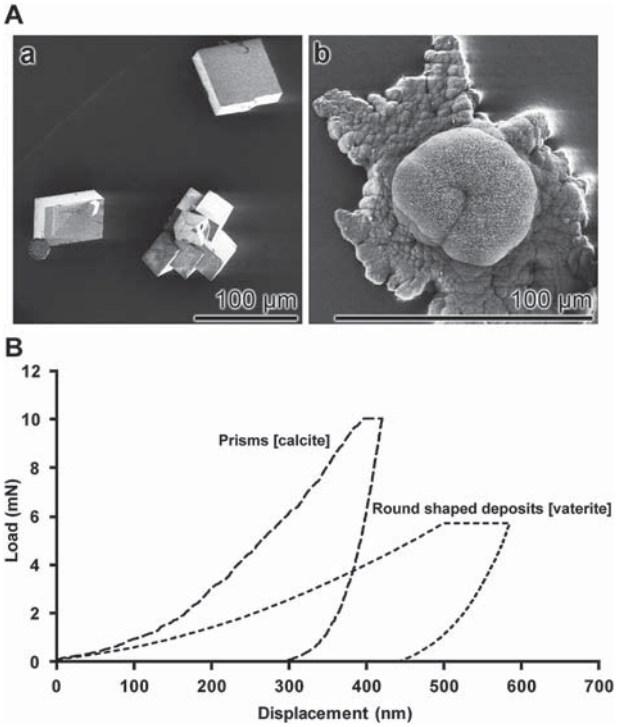

Fig. 4 Mechanical properties of the two forms of Ca-carbonate deposits, synthesized in the "dessicator assay". (A) The properties of the two forms of deposits (a: calcite; and b: vaterite) were measured separately by compiling the respective load–displacement curves applying the indentation technique and applying a Berkovich tip at different forces. SEM. (B) Load–displacement curves obtained from rhombohedral prisms (calcite) and round-shaped deposits (vaterite).

the round-shaped vaterite deposits are shown in Fig. 4B. Applying the Berkovich tip the hardness of the rhombohedral prisms measured 1.98 ± 0.31 GPa, while the hardness of the round-shaped deposits amounts only to 1.38 ± 0.39 GPa. Concurrently, a distinct decrease of the elastic modulus was measured for the round-shaped vaterite deposits (39.13 ± 8.04 GPa), in comparison to the values measured for the rhombohedral calcite prisms (72.83 ± 11.68 GPa). This significant difference in the mechanical properties between the two morphs can also be deduced from the creep behavior. While the creep characteristics for the rhombohedral prisms was found to be 5.44 ± 1.15 (per maximal depth [%]), the corresponding value for the round-shaped vaterite deposits is 9.95 ± 1.60. The increased time-dependent deformation in the round-shaped deposits shows that this vaterite material has a significant (about two-fold) higher viscoplasticity than the rhombohedral prisms.

The two polymorphs of Ca-carbonate deposits can also be distinguished by infrared spectroscopy,[36] using a MIDAC Fourier transform infrared (FT-IR) spectrometer. The data revealed that the rhombohedral prisms show the characteristic vibrational bands for calcite at 873 cm^{-1} and 711 cm^{-1} (Fig. 5A), while the round-shaped deposits show that bands at 875 cm^{-1} and 744 cm^{-1} (Fig. 5B), typical for vaterite.

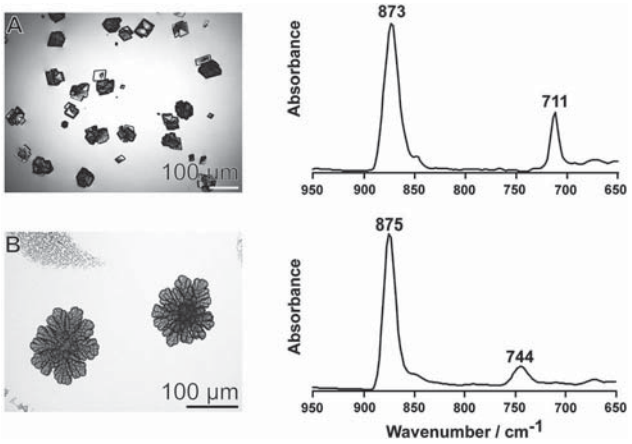

Fig. 5 Infrared spectral analysis of (A) rhombohedral prisms and (B) round-shaped deposits; left panel: LM images; and right panel: FT-IR spectra. (A) The rhombohedral prisms show the characteristic absorption bands of calcite; 873 cm^{-1} and 711 cm^{-1}. (B) The absorption bands of the round-shaped deposits are typical for vaterite; 875 cm^{-1} and 744 cm^{-1}.

3.6. Effect of the D/E-peptide on the kinetics of Ca-carbonate deposition

Addition of CA (35 W-A units per assay) to the Ca-carbonate "dessicator" precipitation assay significantly accelerates the velocity of the Ca-carbonate deposit formation. In the absence of both the CA enzyme and the D/E-peptide the conversion of Ca^{2+} to Ca-carbonate only amounts to 16% after 120 min, while in the presence of CA as much as 65% of Ca^{2+} undergoes carbonate formation (Fig. 6A). In the following 22 h the degree of Ca-carbonate formation increases only slightly, to 75% (Fig. 6A). The D/E-peptide significantly reduces the kinetics of the CA-driven Ca-carbonate precipitation. In the presence of the D/E-peptide, and the absence of the enzyme, the conversion of Ca^{2+} into the insoluble salt measures only 16% Ca-carbonate, while addition of CA strongly accelerates Ca-carbonate formation to 30% (after 120 min), or 55% (after 24 h), respectively (Fig. 6B).

As outlined above rhombohedral calcitic Ca-carbonate deposits are formed in the CA-driven precipitation reaction only in the absence the D/E-peptide (Fig. 3A, B and D; Fig. 4A(a)). In contrast, if the D/E-peptide is added at a concentration of 10 μM to 50 mM $CaCl_2$ only the round-shaped vateritic deposits are produced *in vitro* (Fig. 3A, C and E; Fig. 4A(b)).

The kinetics of Ca-carbonate deposit formation can also be followed by light microscopy. In the absence of the D/E-peptide the rhombohedral crystals start to grow in the CA-containing assay after 30 min reaching a size of 55 ± 12 μm (Fig. 7). During the following incubation period the diameters of the crystals grow to 235 ± 48 μm, after an incubation period of 180 min. In the absence of the enzyme only a few crystals with sizes around 50 μm are formed during the incubation period of 180 min (data not shown).

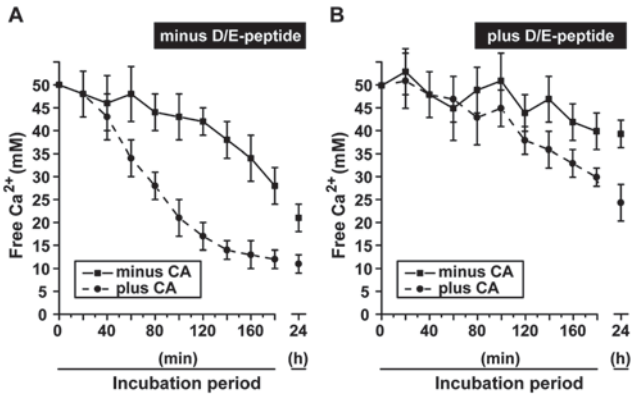

Fig. 6 Increased Ca-carbonate deposit formation in the presence of the enzyme CA. The Ca-carbonate precipitation assay contained 50 mM $CaCl_2$ solution, either in the absence or presence of 35 W-A units per assay of CA. (A) The assays were performed in the absence of the D/E-peptide or (B) presence of 10 μM D/E-peptide. The concentration of free Ca^{2+} was determined by titration. The decrease in the concentration of the free Ca^{2+} concentration reflects the extent of insoluble Ca-carbonate formation. The reactions were performed in the absence (■; solid line) or presence of CA (●; broken line). After terminating the reaction, the samples (six parallel determinations have been performed for each reaction condition) were removed from the assay and then subjected to EDTA titration to determine the remaining free Ca^{2+} concentration. The means ± S.D. are given.

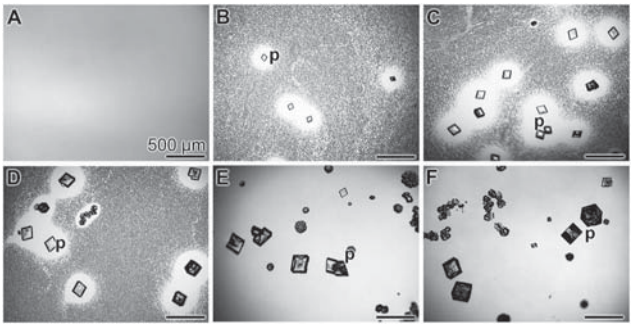

Fig. 7 Time-dependent Ca-carbonate deposit formation in the diffusion assay *in vitro*; LM. The assay contained CA but not the D/E-peptide. The images showing the rhombohedral prisms (p) were taken at time 0 min (A), or 30 min (B), 60 min (C), 90 min (D), 180 min (E), and 300 min (F) of incubation.

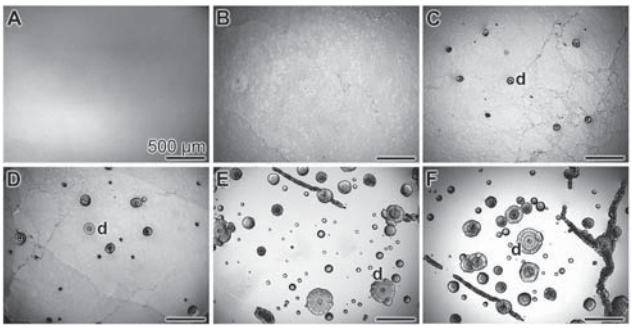

Fig. 8 Formation of round-shaped deposits in the *in vitro* Ca-carbonate deposition assay, supplemented with 10 μM D/E-peptide; LM. Representative images of the areas filled with round-shaped deposits (d) are shown after an incubation period of 0 min (A), 30 min (B), 60 min (C), 90 min (D), 180 min (E), and 300 min (F).

In parallel, the morphology and the abundance of the deposits have been determined in the CA-containing assays in the presence of 10 μM D/E-peptide (Fig. 8). Only round-shaped deposits are formed during the 300 min lasting incubation period. The sizes of the deposits increase from 20 ± 10 μm to 272 ± 196 μm. If the enzyme is omitted from the reactions only very infrequently deposits are visible (data not shown).

4. Discussion

In recent investigations it had been disclosed that the enzyme CA is a key element driving the formation of the calcareous sponge spicules.[17,18] Based on this finding it became possible to approach experimentally the open question for the underlying mechanism(s) which control(s) form/morphology formation of the calcareous spicules and prevent(s) the deposition of biocalcite onto the spicules of the siliceous sponges. It is established that calcareous spicules and siliceous spicules never coexist in the same species, but the siliceous spicules can be associated with massive calcareous skeletons.[37] The present study shows that around the siliceous spicules a protein is located that prevents the enzymatically-controlled calcareous deposit formation. While calcareous crystals are orderly

synthesized and attached to calcareous spicules, here from *S. raphanus*, those crystals do not attach to the surface of the siliceous spicules, like those from *S. domuncula* which had been used in this study. The experiments revealed that the siliceous spicules are covered by the silicatein-associated protein, silintaphin-2.[23] The association of silintaphin-2 with silicatein especially on the surface of the growing siliceous spicules is of importance for guiding the step-wise appositionally layering of the silica lamellae around the spicules.[38] Removal of the silintaphin-2 layer from the *S. domuncula* spicules results in an association of the calcitic crystals to these skeletal elements (to be published). Silintaphin-2 has the distinguished property to act as a Ca^{2+}-binding protein.[23] Among the three Ca^{2+}-binding domains the central one, spanning the aa_{51} to aa_{72} (termed D/E-peptide), is the one which is most acidic (p*I* of 2.99) and comprises the highest abundance of the acidic amino acids, aspartic acid (8 residues) and glutamic acid (4 units) within the 22-mer oligopeptide. Acidic macromolecules are known to be a common component of the organic matrix within mineralized tissues (see: ref. 39). As an example the Asp-rich protein from the shell matrix of the bivalve *Atrina rigida*, accession number AAU04813, can be mentioned;[40] its theoretical p*I* is 2.94. The basic functions of those acidic proteins are not known; it has been postulated that they maintain Ca^{2+} in solution, and by that inhibit the precipitation of Ca-carbonate (reviewed in: ref. 8).

The experiments in the present study show that the D/E-peptide strongly inhibits Ca-carbonate deposit formation in the CO_2 vapor dessicator assay. Under the conditions used the CA-driven Ca-carbonate deposition in the absence of the D/E-peptide results in a rapid (120 min) formation of Ca-carbonate crystals which consist of calcite. In contrast, if the deposits that are synthesized *in vitro* in the presence of the D/E-peptide are analyzed by FT-IR spectrometry only vaterite is found after the same incubation period. The mechanical properties of the Ca-carbonate deposits, of calcite and of vaterite are different. The hardness of the calcite is higher (1.98 ± 0.31 GPa), compared to the vaterite (1.38 ± 0.39 GPa). The reduced elastic modulus of the calcite deposits is significantly lower for vaterite, the round-shaped deposits (39.13 ± 8.04 GPa), compared to the calcite rhombohedral prisms (72.83 ± 11.68 GPa). Furthermore, the determination of the creep characteristics shows higher values for the vaterite deposits ($9.95 \pm 1.60\%$), in comparison to the value for the rhombohedral prisms with $5.44 \pm 1.15\%$.

The D/E-peptide becomes incorporated into the growing Ca-carbonate deposits. This finding implies that the peptide interferes with CO_3^{2-} and Ca^{2+} during Ca-carbonate precipitation. It must be assumed that the calcareous spicules from sponges are likewise synthesized along the energetically downhill sequence from the metastable hydrated ACC *via* less metastable hydrated ACC to the anhydrous ACC from which the CCC phases vaterite, aragonite and finally calcite are formed.[4] Since vaterite is metastable compared to calcite and aragonite, Ca-carbonate monohydrate and vaterite must be prevented from transformation into the stable calcite polymorph by stabilizing physical or (bio)chemical conditions (see: ref. 41). It is the essence of any biological anabolic or catabolic process that the reactions are (mostly) driven by enzymes, *e.g.* in the calcareous sponge spicule system by the CA, at non-saturating and thermodynamically not stable conditions, as seen here for vaterite in the spicular system. With the D/E-peptide, a Ca^{2+}-binding peptide representing a core domain of silintaphin-2, a molecule has been identified that freezes the Ca-carbonate deposits at the unstable vaterite morph.

At present, two explanations can be offered to explain the D/E-peptide-caused freezing of the otherwise unstable vaterite morph. Along with the proposition of Davey *et al.*,[42] it can be assumed that a solution-mediated dissolution of the less stable polymorph, here vaterite, is followed by the nucleation of the stable polymorph, here calcite. However, this transformation route appears to be unlikely since the vaterite crystals formed in the presence of the D/E-peptide are stable even after 20 days (not shown here), indicating that the vaterite phase is kinetically stabilized by the D/E-peptide. The second mechanism which appears to be the most likely one is a strong interaction of the D/E-peptide with the vaterite *via* Ca–O bonds that prevents the dissolution of vaterite particles. A further possibility, a solid-state transformation during which an internal rearrangement of the lattice occurs, requires further Raman spectral analyses of the Ca-carbonate crystals. It is well established that other proteins, *e.g.* ovalbumin[43] can stabilize the metastable vaterite phase. However, the concentrations of those organic template used, *e.g.* for ovalbumin with 2 g L^{-1}, are considerably higher than the concentration required for the D/E-peptide to stabilize the vaterite phase with 30 mg L^{-1} in present study. This comparison reflects the high specificity and the high selectivity of the D/E-peptide by which it acts during the course of vaterite/Ca-carbonate biomineralization. Likewise, also metal ions are known to block phase-specific calcite formation.[44]

Vaterite (hexagonal dihexagonal dipyramidal crystals), aragonite (orthorhombic) and calcite (rhombohedral) have the same chemical composition, but besides of the different crystal structure of the CO_3^{2-} ions, a different coordination environment of Ca^{2+}. As the calcium atoms have a six-fold coordination in calcite and a nine-fold in aragonite, the calcium atoms in vaterite have an eight-fold coordination (see: ref. 45), it can be deduced that the D/E-peptide recognizes the degree of packaging of the Ca^{2+} within the crystal structures. The effect of the D/E-peptide on the transformation/freezing of the Ca-carbonate morph vaterite is strong. Already at a low molar ratio of D/E-peptide : Ca^{2+} of 1 : 5000, a pronounced vaterite freezing effect occurs. This finding suggests that the stabilization of the vaterite morph caused by the D/E-peptide is due not only to a cooperative influence between the organic and the inorganic components of the system,[46] but also to a nucleating/stabilizing effect of the D/E-peptide-stabilized vaterite crystals on the formation/growth of new peptide-lacking vaterite crystals. However, it is more likely that one D/E-peptide is sufficient to induce the formation of vaterite nano-crystals, ranging from 30 nm to 250 nm,[47] that are build of around 5×10^6 Ca-carbonate molecules.

5. Conclusion

The results presented in this study provide a first step towards the elucidation of the taxon-specific skeletal-element

formation/rejection. Future studies, directed towards a biotechnological application of the D/E-peptide-controlled Ca-carbonate deposition applying the CA-driven precipitation reaction, will focus on the effect of silicate on the two-component microstructures, composed of the D/E-peptide and vaterite. It has been described that silicate ions accelerate the Ca-carbonate deposition in the presence of proteins, *e.g.* casein.[48] Further applications of vaterite, especially if it is applied for surface coatings, for functionalization with inorganic or organic ligands and also for changing the degree of hydrophobicity, can be anticipated.

Acknowledgements

W.E.G. M. is a holder of an ERC Advanced Investigator Grant (no. 268476 "BIOSILICA"). D. P. is a holder of an ERC Starting Investigator Grant (no. 306357 "NANO-JETS"). The support from the Apulia Regional Projects 'Networks of Public Research Laboratories' Wafitech (9) and M. I. T. T. (13) is also acknowledged. This work was supported by grants from the German Bundesministerium für Bildung und Forschung (project "Center of Excellence BIOTECmarin"), the Deutsche Forschungsgemeinschaft (SCHR 277/10-2), the European Commission (Seventh Framework Programme, Marie-Curie Initial Training Network "BIOMINTEC", Grant no. 215507; and Industry-Academia Partnerships and Pathways "CoreShell"; Grant no. 286059), and the International Human Frontier Science Program.

Notes and references

1 V. v. Ebner, *Über den feineren Bau der Skelettheile der Kalkschwämme nebst Bemerkungen über Kalkskelete überhaupt*, Gerold, Wien, 1887.
2 O. B. Bøggild, *The Shell Structure of the Mollusks*, Andr. Fred. Høst, København, 1930.
3 E. Haeckel, *Die Radiolarien (RHIZOPODA RADIARIA)*, Georg Reimer, Berlin, 1862.
4 A. V. Radha, T. Z. Forbes, C. E. Killian, P. U. P. A. Gilbert and A. Navrotsky, *Proc. Natl. Acad. Sci. USA*, 2010, **107**, 16438–16443.
5 L. Addadi, S. Raz and S. Weiner, *Adv. Mater.*, 2003, **15**, 959–970.
6 M. J. Uriz, *Can. J. Zool.*, 2006, **84**, 322–356.
7 I. Sethmann and G. Wörheide, *Micron*, 2008, **39**, 209–228.
8 F. Marin, N. Le Roy and B. Marie, *Front. Biosci., Scholar Ed.*, 2012, **4**, 1099–1125.
9 W. E. G. Müller, X. H. Wang, V. A. Grebenjuk, M. Korzhev, M. Wiens, U. Schloßmacher and H. C. Schröder, *PLoS ONE*, 2012, **7**, e34617.
10 W. E. G. Müller, A. Maidhof, R. K. Zahn and I. Müller, *Coral Reefs*, 1983, **1**, 237–241.
11 S. Tambutté, E. Tambutté, D. Zoccola, N. Caminiti, S. Lotto, A. Moya, D. Allemand and J. Adkins, *Mar. Biol.*, 2006, **151**, 71–83.
12 M. A. Ocaña, J. M. Tierno de Figueroa and R. J. Palomino-Morales, *Zool. Sci.*, 2006, **23**, 557–564.
13 X. H. Wang, H. C. Schröder, K. Wang, J. A. Kaandorp and W. E. G. Müller, *Soft Matter*, 2012, **8**, 9501–9518.
14 W. E. G. Müller, H. C. Schröder, Z. Burghard, D. Pisignano and X. H. Wang, *Chem.–Eur. J.*, 2013, **19**, 5790–5804.
15 H. C. Schröder, X. H. Wang, A. Manfrin, S. H. Yu, V. A. Grebenjuk, M. Korzhev, M. Wiens, U. Schloßmacher and W. E. G. Müller, *J. Biol. Chem.*, 2012, **287**, 22196–22205.
16 X. H. Wang, H. C. Schröder, D. Brandt, M. Wiens, I. Lieberwirth, G. Glasser, U. Schloßmacher, S. F. Wang and W. E. G. Müller, *ChemBioChem*, 2011, **12**, 2316–2324.
17 W. E. G. Müller, U. Schlossmacher, H. C. Schröder, I. Lieberwirth, G. Glasser, M. Korzhev, M. Neufurth and X. H. Wang, *Acta Biomater.*, 2014, **10**, 450–462.
18 W. E. G. Müller, H. C. Schröder, U. Schlossmacher, M. Neufurth, W. Geurtsen, M. Korzhev and X. H. Wang, *FEBS Open Bio*, 2013, **3**, 357–362.
19 J. Aizenberg, D. A. Muller, J. L. Grazul and D. R. Hamann, *Science*, 2003, **299**, 1205–1208.
20 J. Aizenberg, M. Ilan, S. Weiner and L. Addadi, *Connect. Tissue Res.*, 1996, **34**, 255–261.
21 L. Addadi and S. Weiner, *Proc. Natl. Acad. Sci. U.S.A.*, 1985, **82**, 4110–4114.
22 H. Tong, W. Ma, L. Wang, P. Wan, J. Hu and L. Cao, *Biomaterials*, 2004, **25**, 3923–3929.
23 M. Wiens, H. C. Schröder, X. H. Wang, T. Link, D. Steindorf and W. E. G. Müller, *Biochemistry*, 2011, **50**, 1981–1990.
24 G. LePennec, S. Perović, M. S. A. Ammar, V. A. Grebenjuk, R. Steffen and W. E. G. Müller, *J. Biotechnol.*, 2003, **100**, 93–108.
25 W. E. G. Müller, X. H. Wang, V. A. Grebenjuk, M. Korzhev, M. Wiens, U. Schloßmacher and H. C. Schröder, *Biochem. J.*, 2012, **448**, 233–242.
26 D. Wang, A. F. Wallace, J. J. De Yoreo and P. M. Dove, *Proc. Natl. Acad. Sci. U.S.A.*, 2009, **106**, 21511–21516.
27 E. J. Slowinski, W. C. Wolsey and W. L. Masterton, *Chemical principles in the laboratory*, Brooks/Cole, Belmont, CA, 9th edn, 2009.
28 W. E. G. Müller, X. H. Wang, B. Diehl-Seifert, K. Kropf, U. Schloßmacher, I. Lieberwirth, G. Glasser, M. Wiens and H. C. Schröder, *Acta Biomater.*, 2011, **7**, 2661–2671.
29 N. V. Vagenas, A. Gatsouli and C. G. Kontoyannis, *Talanta*, 2003, **59**, 831–836.
30 W. C. Oliver and G. M. Pharr, *J. Mater. Res.*, 1992, **7**, 1564–1583.
31 S. Compton and C. G. Jones, *Anal. Biochem.*, 1985, **151**, 369–374.
32 L. Sachs, *Angewandte Statistik*, Springer, Berlin, 1984, p. 242.
33 T. Liu and R. B. Altman, *BMC Struct. Biol.*, 2009, **9**, 72.
34 M. Fändrich, V. Forge, K. Buder, M. Kittler, C. M. Dobson and S. Diekmann, *Proc. Natl. Acad. Sci. U.S.A.*, 2003, **100**, 15463–15468.
35 A. Lewit-Bentley and S. Réty, *Curr. Opin. Struct. Biol.*, 2000, **10**, 637–643.
36 P. U. P. A. Gilbert and F. H. Wilt, in *Molecular Biomineralization, Progress in Molecular and Subcellular Biology*, ed. W. E. G. Müller, Springer, Heidelberg, 2011, vol. 52, pp. 199–223.
37 R. Garrone, T. L. Simpson and J. Pottu-Boumendil, in *Silicon and Siliceous Structures in Biological Systems*, ed. T. L.

Simpson and B. E. Volcani, Springer, Heidelberg, 1981, pp. 495–525.
38 H. C. Schröder, A. Boreiko, M. Korzhev, M. N. Tahir, W. Tremel, C. Eckert, H. Ushijima, I. M. Müller and W. E. G. Müller, *J. Biol. Chem.*, 2006, **281**, 12001–12009.
39 H. A. Lowenstam and S. Weiner, *On Biomineralization*, Oxford University Press, New York, 1989.
40 B. A. Gotliv, N. Kessler, J. L. Sumerel, D. E. Morse, N. Tuross, L. Addadi and S. Weiner, *ChemBioChem*, 2005, **6**, 304–314.
41 F. C. Meldrum and H. Cölfen, *Chem. Rev.*, 2008, **108**, 4332–4432.
42 R. J. Davey, P. T. Cardew, D. McEwan and D. E. Sadler, *J. Crystal Growth*, 1986, **79**, 648–653.
43 X. Wang, R. Kong, X. Pan, H. Xu, D. Xia, H. Shan and J. R. Lu, Role of ovalbumin in the stabilization of metastable vaterite in calcium carbonate biomineralization, *J. Phys. Chem. B*, 2009, **113**, 8975–8982.
44 K. Naka and Y. Chujo, Control of crystal nucleation and growth of calcium carbonate by synthetic substrates, *Chem. Mater.*, 2001, **13**, 3245–3259.
45 J. Wang and U. Becker, *Am. Mineral.*, 2009, **94**, 380–386.
46 L. Addadi, J. Moradian, E. Shay, N. G. Maroudas and S. Weiner, *Proc. Natl. Acad. Sci. U.S.A.*, 1987, **84**, 2732–2736.
47 J. Ahmed, M. Ganguli and A. K. Ganguli, *CrystEngComm*, 2009, **11**, 927–932.
48 A. E. Voinescu, D. Touraud, A. Lecker, A. Pfitzner, L. Kienle and W. Kunz, *J. Phys. Chem. C*, 2008, **112**, 17499–17506.